Zwitterionic targeting doxorubicin-loaded micelles assembled by amphiphilic dendrimers with enhanced antitumor performance

Lu Zhang[a], Quanling Guo[a], Ruixue Zheng[a], Qingyu Yu[b], Ying Liang[a], Guanglong Ma[c], Qiurong Li[a], Xiaoyu Zhang[a], Haiyan Xiao[a], Longgang Wang[a]**

a. *State Key Laboratory of Metastable Materials Science and Technology, Hebei Key Laboratory of Nano-biotechnology, Hebei Key Laboratory of Applied Chemistry, Yanshan University, Qinhuangdao, 066004, China*

b. *School of Chemical Engineering and Technology, Tianjin University, Tianjin, 300072, China*

c. *Centre for cancer immunology, Faculty of medicine, University of Southampton, Southampton, SO166YD, UK*

* *Corresponding author:* Xiaoyu Zhang, Longgang Wang

Abstract

Chemotherapy is the main method of treating malignant tumors in clinical treatment. However, the commonly used chemotherapeutic drugs have the disadvantages of high biological toxicity, poor water solubility, low targeting ability, and high side effects. Zwitterionic micelles assembled by amphiphilic dendrimers modified with zwitterionic groups and targeting ligand should largely overcome these shortcomings. Herein, the zwitterionic group and targeting peptide c(RGDfC) were modified on the surface of generation 2 poly (propylene imine) dendrimers (G2 PPI), which was conjugated with hydrophobic N-(2-mercaptoethyl) oleamide to form amphiphilic dendrimers (PPIMYRC). PPIMYRC self-assembled into micelles with doxorubicin (DOX) loaded in the interior of micelles to prepare DOX-loaded micelles (PPIMYRC-DOX micelles). The PPIMYRC-DOX micelles had great stability in fibrinogen and pH responsive drug release. Furthermore, PPIMYRC-DOX micelles had higher cellular uptake rates than free DOX, resulting in higher cytotoxicity of PPIMYRC-DOX micelles than that of free DOX. More importantly, PPIMYRC-DOX micelles inhibited tumors much better than free DOX. The tumor inhibition rate of PPIMYRC-DOX micelles was as high as 93%. Taken together, PPIMYRC-DOX micelles were assembled by amphiphilic dendrimers with the zwitterionic and targeting groups, which enhanced the therapeutic effect of DOX and reduced its side effects. The prepared targeting nanodrug has great potential for further application in antitumor therapy.

KEYWORDS: doxorubicin, dendrimer, c(RGDfC), drug delivery, zwitterionic

1. INTRODUCTION

Cancer is a major global problem with high morbidity and high mortality, which has brought a huge burden to society.[1-3] Right now, chemotherapy is the main method of clinical treatment of cancer[4,5] especially the treatment of malignant tumors and systemic metastatic cancers. However, traditional chemotherapeutic drugs like paclitaxel (PTX)[6], doxorubicin (DOX)[7] and camptothecin (CPT) [8] are small molecule drugs and have many limitations. For example, these small molecule drugs generally have poor water solubility, poor tumor targeting ability and high toxicity [9]. Researchers have developed a number of drug delivery systems (DDSs) to overcome these shortcomings of traditional small molecule drugs,[10,11] such as liposomes,[12] peptides,[13,14] polymer micelles,[15] and dendrimers.[16,17] These DDSs reduce drug toxicity and improve drug utilization by enhancing permeability and retention (EPR) effects.[18,19]

Polymer micelles have good application prospects in nanomedicine.[20] Polymeric micelles improve water solubility of hydrophobic small molecule drugs and controlled release at tumor sites. However, they are easily recognized non-specifically by proteins in the blood through intravenous injection and removed from the body by the reticuloendothelial system (RES),[21,22] which largely reduces the efficiency of drug-loaded polymer micelles in delivering small molecule drugs to tumors. The modification of polyethylene glycol (PEG) on the surface of polymer micelles will improve the blood circulation time of polymer micelles. However, PEG has many drawbacks including generation antibodies and weak interaction with proteins, resulting in reduced therapeutic efficacy.[23,24] Therefore, how to improve the

biocompatibility of polymer micelles and the delivery efficiency of small molecule anticancer drugs has become the focus of the treatment of cancer.

Since zwitterionic materials can form a dense hydration layer in water, prevent direct contact with proteins, and reduce interaction with proteins, they have good performance of reducing non-specific protein adsorption.[25,26] Zwitterionic groups are modified on the polymer to prepare zwitterionic polymers, which improves the protein stability of polymer micelles and the delivery efficiency of small molecule anticancer drugs.[27,28] However, the number of zwitterionic groups modified on the polymer is uncontrollable,[29,30] and too many zwitterionic groups of polymer micelles make them difficult to enter into the tumor site.[31] Dendrimers have controllable surface modification sites and good water solubility. The amphiphilic dendrimers micelles have the merits of dendrimers and can achieve controlled drug release.[32] In addition, the passive targeting depends on the vascular defects at the tumor site and has selective high enhanced permeability and retention effect (EPR effect) to macromolecular substances and lipid nanoparticles,[33,34] the receptor mediated active targeting delivery system has further improved the anti-tumor effect of nanodrug. Integrin $\alpha_v\beta_3$ is overexpressed in a variety of tumor cells,[35] and short zwitterionic peptide c(RGDfC) can selectively recognize and bind integrin $\alpha_v\beta_3$ with high affinity. [36,37] Therefore, we designed to modify ligand c(RGDfC) on nanodrug carriers to achieve active targeting and achieve better anti-tumor effect.

In this paper, a new kind of amphiphilic dendrimers (PPIMYRC) was synthesized, where generation 2 polypropylene imine dendrimer (G2 PPI) with zwitterionic groups and c(RGDfC) ligand was used as the hydrophilic end, and the linear molecule N-(2-mercaptoethyl) oleamide was used as the hydrophobic end. PPIMYRC nanomicelles formed by self-assembly and encapsulated DOX by physical entrapment to prepare zwitterionic targeting DOX-loaded micelles (PPIMYRC-DOX micelles). The zwitterionic shell of PPIMYRC-DOX micelles made them have good dispersion and

stability. PPIMYRC-DOX micelles accumulated at the tumor through EPR effect, and the targeting ligand c(RGDfC) enabled PPIMYRC-DOX micelles to target tumor cells and be endocytosed by tumor cells. In cell experiments, fluorescence microscopy and flow cytometry were used to explore the reason of the high cytotoxicity of PPIMYRC-DOX micelles. In addition, PPIMYRC-DOX micelles had a good tumor-inhibiting effect. Therefore, we provide a new carrier with targeted and controlled drug release for enhanced antitumor effect.

2. Experimental section

2.1 Materials

Materials were in supporting information.

2.2 Synthesis of zwitterionic dendrimer

Detailed synthesis steps and dosages are provided in the supporting information. G2 PPI and maleic anhydride in DMSO were reacted to obtain the product maleic anhydride modified G2 PPI (PPIM). N-(2-mercaptoethyl) oleamide and PPIM were dissolved in CH_2Cl_2 and CH_3OH, respectively. Then they were mixed and reacted to obtain product N-(2-mercaptoethyl) oleamide modified PPIM (PPIMY). PPIMY and c(RGDfC) were mixed and reacted in CH_3OH to obtain product c(RGDfC)modified PPIMY (PPIMYR). Cysteamine and PPIMYR in CH_3OH were reacted to obtain the product cysteamine modified PPIMYR (PPIMYRC). The steps of synthesis are shown in **Figure 1**.

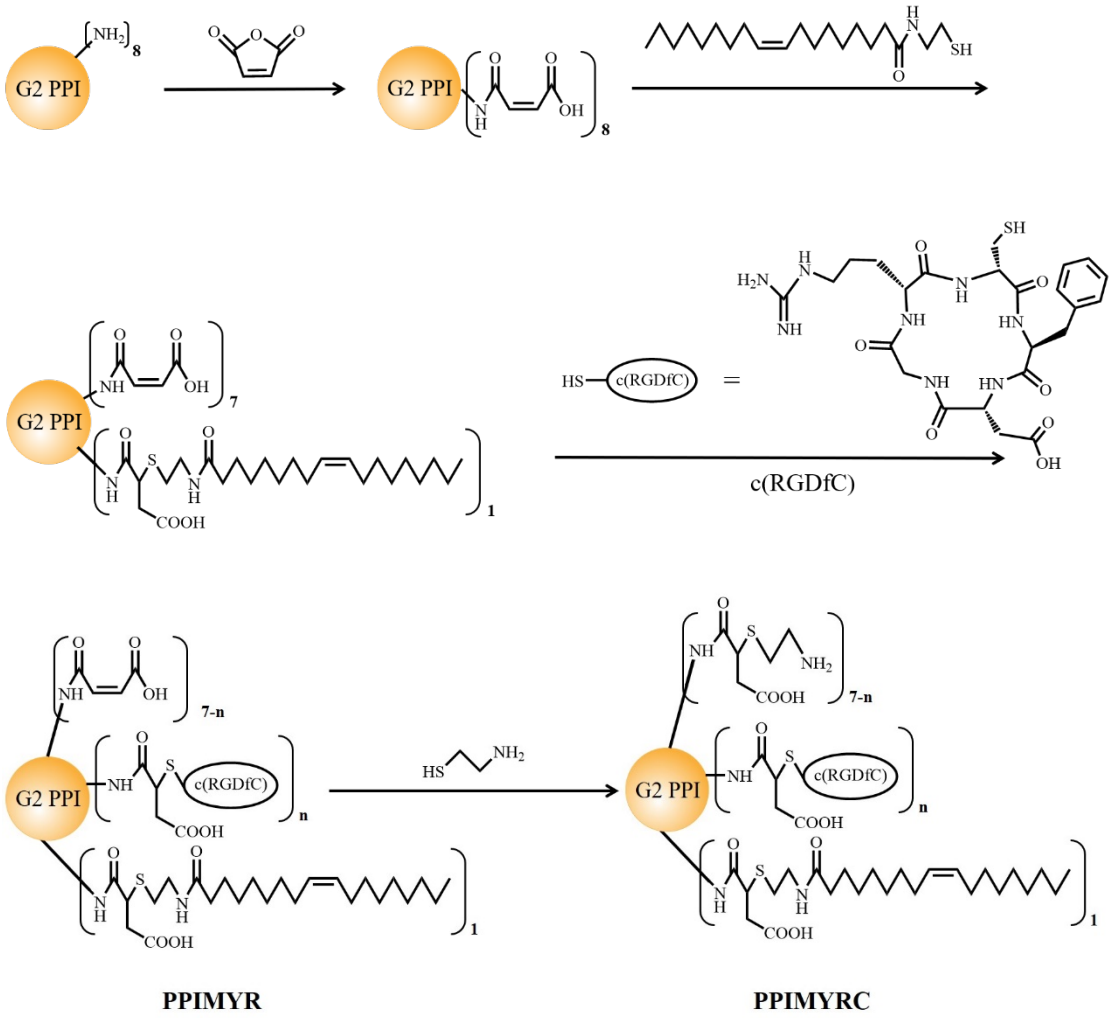

Figure 1. The synthesis steps of PPIMYRC

2.3 Preparation of drug-loaded micelles

DOX·HCl and triethylamine were dissolved in CH_3OH, then sonicated in the dark for 1 h to obtain DOX solution in CH_3OH. PPIMYRC was dissolved in 1 mL of CH_3OH. DOX and PPIMYRC were mixed and reacted for 3 h in dark. The solution after the reaction was slowly dropped into 1.5 mL of water at a rate of 1 mL/min, and then the mixed solution was dialyzed in H_2O to obtain DOX-loaded micelles (PPIMYRC-DOX micelles). The data of drug-loaded micelles were calculated by the formulas:

$$\text{Drug loading efficiency (DLE)} = \frac{\text{mass of DOX in micelles}}{\text{total mass of micelles}} \times 100 \qquad 1$$

$$\text{Encapsulation efficiency (EE)} = \frac{\text{mass of DOX in micelles}}{\text{total mass of DOX added}} \times 100 \qquad 2$$

2.4 Characterization

PPIMYRC-DOX micelles were dissolved in different pH deionized water (7.4, 6.5, and 5.5) at a concentration of 1 mg/mL. Fibrinogen, PPIMYRC micelles, and PPIMYRC-DOX micelles were dissolved phosphate buffer saline (PBS) at pH 7.4 to simulate a human normal environment. The hydrodynamic size, zeta potential as well as protein stability of the samples were measured by DLS.

2.5 Drug release assay

The PPIMYRC-DOX micelles solution (C_{DOX} = 20 μg/mL) was dialyzed against PBS solutions of different pH values (pH = 5.5, 6.5 and 7.4). 1.5 mL of fresh PBS solution was used to replace the old PBS solution every 30 min. Finally, the fluorescence intensity of each sample at E_x=480 nm was measured with the fluorescence spectrophotometer.

2.6 Cytotoxicity assay

The MTT analysis was used for examining the biocompatibility of PPIMYRC to cells. HeLa and A549 cells were plated in 96-well plates (1×10^4 cells/well), respectively. 24 h latter, a new DMEM medium containing 27.5-440 μg/mL PPIMYRC and G2 PPI was employed to replace the original medium, respectively. Another 24 h latter, 100 μL of MTT solution per well was substituted for the original medium. The solution of MTT was replaced by 150 μL of DMSO per well after 4 h. Afterwards, the microplate reader was used for measuring the absorbance of the sample at 490 nm. Besides, the cytotoxicity of PPIMYRC-DOX micelles to A549 and HeLa cells was determined in

the same way.

2.7 Cellular uptake assay

Confocal microscopy was applied to qualitatively analyze cellular uptake of DOX and PPIMYRC-DOX micelles. A549 cells were plated in a 24-well plate (1×10^5 cells/well). The DMEM with DOX and PPIMYRC-DOX micelles (C_{DOX}=5 μg/mL) replaced the previous medium. After 20 h, cell nuclei was stained with Hoechest 3342, and confocal microscopy was used to photograph the cells.

A549 cells were plated in a 6-well plate (1×10^5 cells/well). The previous solution was replaced with DMEM containing free DOX and PPIMYRC-DOX micelles (C_{DOX}=5 μg/mL) with different pH (5.5, 6.5, 7.4). After 20 h, cells were collected. Finally, the flow cytometry was applied to measure the fluorescence intensity of DOX. The flowjo10.0 program was used to analyze the experimental data.

2.8 Antitumor assay *in vivo*

The female KM mice were randomly divided into 4 groups: saline group, free DOX group, PPIMYRC micelles group and PPIMYRC-DOX micelles group. Each group had 6 mice. Each mouse was injected with 200 μL of sample at a time by tail vein injection, and they were injected 7 times (C_{DOX}=2.5 mg/kg) (mass of DOX/mouse body weight). Various data of mice were recorded during dosing. The tumor volume was calculated with formula 3:

$$V = \frac{a\times b^2}{2} \quad (3)$$

V means the tumor volume, a is the long diameter of tumor, b is the short diameter of tumor.

The tumor inhibition rate was calculated with formula 4:

$$Tumor\ inhibition\ rate = \frac{V_{control} - V_{experitmental}}{V_{control}} \times 100 \quad (4)$$

After 14 days, the main organs were collected. The damage of the samples to the major organs and tissues of mice was detected by H&E staining. Furthermore, to reveal the liver impairment of mice, the levels of alanine aminotransferase (ALT) and aspartate aminotransferase (AST) in the blood was tested through standard kits.

2.9 Statistical analysis

Data were shown as mean ± SD. Statistical significance was determined by one-way anova (*P<0.05)

3. Results and discussion

3.1 Synthesis of PPIMYRC

PPIMYRC-DOX micelles were prepared through the self-assembly of amphiphilic dendrimers PPIMYRC with physical entrapment in DOX. **Figure 2A** shows the ^{1}H NMR spectra of PPIM in D_2O and PPIMYRC, PPIMYR and PPIMY in mixed solvent of D_2O and CD_4O (V_{D2O}: V_{CD4O} =1:1). Compared with PPIM, there were three new peaks in the PPIMY spectrum at chemical shifts 5.34, 1.30 and 0.88 ppm, which were the characteristic peaks of N-(2-mercaptoethyl) oleamide. This result proved that PPIMY was successfully synthesized. A new peak appeared in the PPIMYR spectrum at a chemical shift of 7.25 ppm, which was generated by the H on the benzene ring in c(RGDfC), which proved the successful synthesis of PPIMR. The ^{1}H NMR spectrum of c(RGDfC) is shown in **Figure S1**. In the PPIMYRC spectrum, there were two peaks completely disappeared at the chemical shifts of 6.25 and 5.84 ppm, which indicated

that a small part of the remaining double bonds on the PPIMYR were completely reacted, proving the successful synthesis of the target product PPIMYRC.

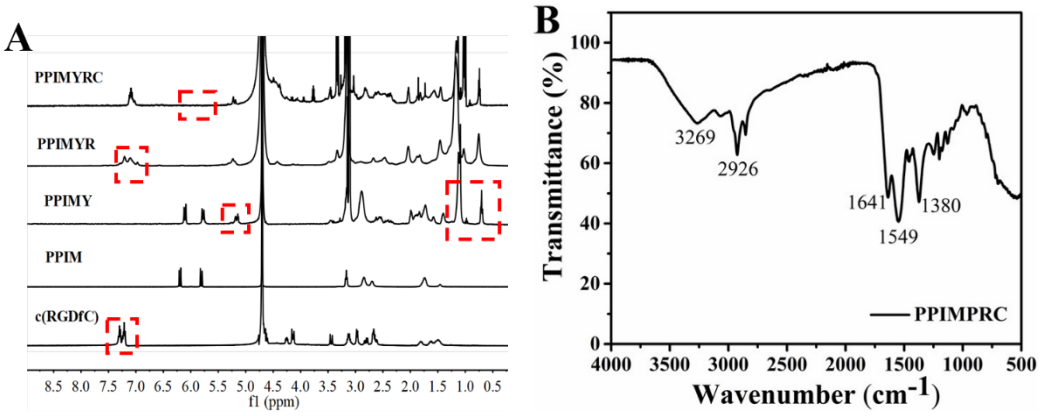

Figure 2. (A) ^{1}H NMR spectra of PPIM in D_2O and PPIMYRC, PPIMYR and PPIMY in mixed solvent of D_2O and CD_4O (V_{D2O}: V_{CD4O} =1:1), (B) infrared absorption spectrum of PPIMYRC

Infrared spectroscopy was used to prove the successful synthesis of PPIMYRC. As shown in **Figure 2B**, the absorption peak at 3269 cm^{-1} comes from N-H stretching vibration. The absorption peak at 2926 cm^{-1} comes from the stretching vibration of O-H in carboxyl group. The absorption peak at 1641 cm^{-1} comes from the stretching vibration of C=C. The absorption peaks of 1549 cm^{-1} and 1380 cm^{-1} come from the stretching vibration of benzene ring skeleton and methyl group, respectively. The infrared spectrum of PPIMYRC is consistent with its molecular formula, which proves the successful synthesis of PPIMYRC. **Figure S2** shows that the number average molecular weight of PPIMYRC is 767 Da on the elution curve. This value is lower than the calculated value because the dendrimer has a three-dimensional spherical structure, and the hydrodynamic radius of spherical molecules is much smaller than that of linear polymers with the same molecular weight, so the experimental value is lower than the

calculated value.

3.2 Characterization of PPIMYRC-DOX micelles

To verify that PPIMYRC-DOX micelles successfully encapsulated DOX, the UV-Vis spectrophotometer was used to measure whether there were peak shifts. As shown in **Figure 3A**, 480 nm and 495 nm are the characteristic absorption peaks of DOX and PPIMYRC-DOX, respectively. The characteristic absorption peaks of PPIMYRC-DOX micelles were provided by DOX. The comparison showed that the position of the characteristic absorption peak of DOX in PPIMYRC-DOX micelles was red-shifted. This was the result of DOX being encapsulated into the hydrophobic core of PPIMYRC-DOX micelles, proving that DOX packaging was successful.[38] Furthermore, the color of three samples in **Figure 3B** further confirmed this result. The DLE and EE of PPIMPC-DOX micelles were 5.7% and 37.2%, respectively. Therefore, PPIMYRC-DOX micelles successfully encapsulated DOX in their core.

The size and morphology of micelles affected the interaction between cells and nanoparticles.[39] The PPIMYRC-DOX micelles were dropped on the copper mesh support film, and the phosphotungstic acid was used for negative dyeing. The morphology and particle size of PPIMYRC-DOX micelles was characterized by TEM.[40] As displayed in **Figure 3C**, the morphology of PPIMYRC-DOX micelles was irregularly spherical. As displayed in **Figure 3D**, the particle size distribution histogram displayed that the average particle size of PPIMYRC-DOX micelles was 21.5 nm, which proved PPIMYRC-DOX micelles had small particle size and narrower particle size distribution. Spherical structure facilitated penetration and enrichment of micelles

at tumor sites.[41] The TEM characterization showed that PPIMYRC-DOX micelles had the potential to be enriched in the tumor site through the EPR effect.[42]

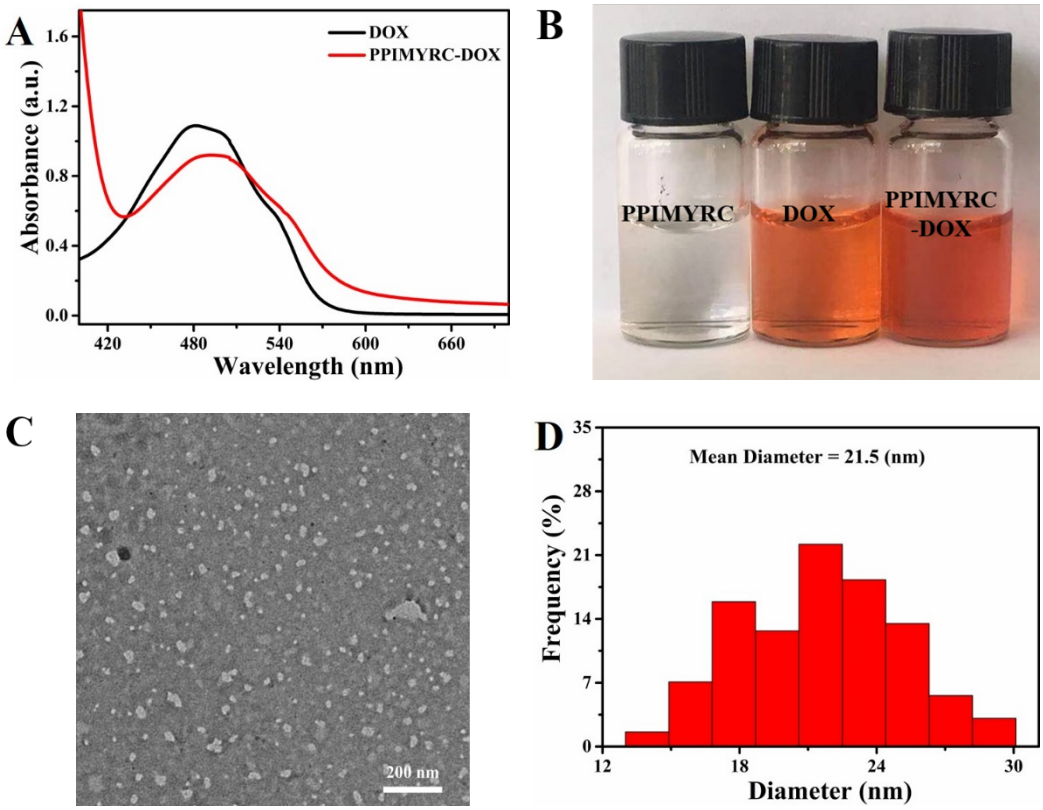

Figure 3. (A) UV-Vis spectra of DOX and PPIMYRC-DOX micelles, (B) pictures of PPIMYRC micelles, DOX and PPIMYRC-DOX micelles, (C) TEM image and (D) particle size distribution histogram of PPIMYRC-DOX micelles

The zeta potential and hydrodynamic size played an important role in nano-drug delivery.[43-45] The effect of different pH on the zeta potential and hydrodynamic size was studied with DLS method. As depicted in **Figure 4A**, the hydrodynamic size of PPIMYRC-DOX micelles was 38.7, 58.9 and 69.2 nm for pH 5.5, 6.5 and 7.4, respectively. The hydrodynamic size of PPIMYRC-DOX gradually increased with decreasing pH. PPIMYRC-DOX micelles with small hydrodynamic size can improved drug accumulation at tumor sites by EPR effect. In an acidic environment, the

hydrodynamic size of PPIMYRC-DOX gradually got bigger with increasing concentration of H^+. This was due to the protonation of the amino groups and carboxylate group on the surface of the PPIMYRC-DOX micelles and the increasing electrostatic repulsion in them.[46] This result proved that PPIMYRC-DOX micelles had a certain pH responsiveness and the potential to release drugs at the tumor site.[47]

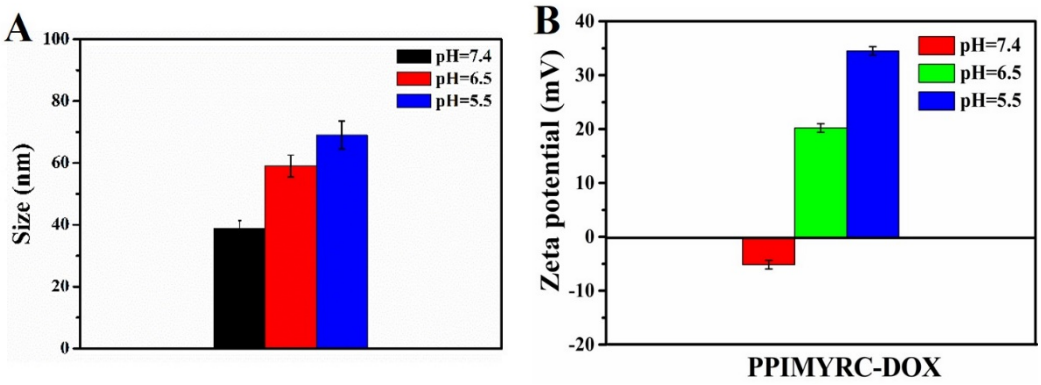

Figure 4. (A) Hydrodynamic size and (B) corresponding zeta potential of PPIMYRC-DOX micelles at different pH

It was further determined that the zeta potential of PPIMYRC-DOX was affected by pH. As depicted in **Figure 4B**, the zeta potential of PPIMYRC-DOX was -5.2, 20.2 and 34.5 mV in deionized water at pH 7.4, 6.5 and 5.5, respectively. PPIMYRC-DOX micelles showed slightly negative charge at pH 7.4, indicating they had zwitterionic states, which was favorable for the good stability of PPIMYRC-DOX in protein solutions. With the decrease of pH, the protonation of the amino groups and carboxylate group on the surface of PPIMYRC-DOX micelles were happened under acidic conditions, resulting in the reversal of the surface charge of PPIMYRC-DOX micelles. The zeta potential of PPIMYRC-DOX micelles changed from negative to positive charges at the tumor site, which was conducive to improving the uptake of PPIMYRC-

DOX micelles by cells, thereby improving the therapeutic effect of tumors.[48]

3.3 Protein stability

When the drug-loaded micelles were injected into the body, they encounter many proteins in the blood. Strong interactions between drug-loaded micelles and proteins can lead to their coagulation and reduce blood circulation time. Therefore, the drug-loaded micelles should have good protein stability before drug-loaded micelles were injected into the body to inhibit tumors. Therefore, the stability of PPIMYRC and PPIMYRC-DOX micelles in protein solution was measured. **Figure 5A** shows the hydrodynamic size of 1 mg/mL PPIMYRC micelles and 0.5 mg/mL fibrinogen were 8.8 and 23.0 nm, respectively. And the hydrodynamic size of the mixed solution was in the middle of them. The hydrodynamic size of 1 mg/mL PPIMYRC-DOX micelles was 56.5 nm, the hydrodynamic size of the mixed solution was between them in **Figure 5B**. The experimental results proved that PPIMYRC micelles and PPIMYRC-DOX micelles had no obvious aggregation phenomenon when they incubated with fibrinogen, they can form a stable mixed solution, which proved that PPIMYRC-DOX micelles had good stability. The reason was that the zwitterionic PPIMYRC and PPIMYRC-DOX micelles can form a dense water film on their surface to prevent direct contact with proteins.

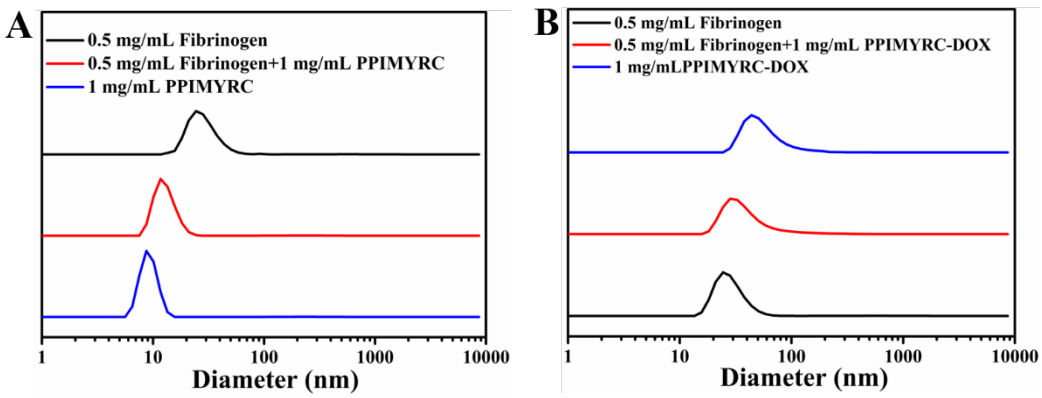

Figure 5. The protein stability of (A) PPIMYRC micelles and (B) PPIMYRC-DOX micelles in fibrinogen solution in PBS at pH=7.4

3.4 Release of DOX from PPIMYRC-DOX micelles

An important way to improve the effect of tumor treatment was to increase the concentration of the drug at the tumor site. Therefore, the release profile of small molecule drugs is particularly important in nano-drug delivery systems. It is required that the drug-loaded micelles have no sudden release under normal physiological environment, thereby reducing the toxic and side impacts of anti-cancer drugs on normal tissues.[49] Generally, the pH in tumor sites is lower than normal tissues. Therefore, micelles were triggered drug release in a low pH environment, which can accelerate the release of drugs at tumor sites, showing a good application prospect for nanomedicine.

A fluorescence spectrophotometer was applied to analyze the DOX release behavior of PPIMYRC-DOX micelles at different pH. The normal physiological environment, early endosomes and lysosomes were simulated by PBS solutions with different pH values (pH = 7.4, 6.5, 5.5), respectively. The release of DOX was studied in the above

solution. The cumulative drug release of PPIMYRC-DOX micelles in the PBS at pH=7.4, 6.5, and 5.5 were 17.0%, 29.9%, and 58.5% after 30 h in **Figure 6**, respectively. By comparison, it was found that there was no sudden release of DOX in PBS solutions at different pH, which indirectly indicated that PPIMYRC-DOX micelles can reduce the damage of free DOX to the normal tissue *in vivo*. With the pH decreased, the cumulative release of DOX gradually increased. The experiments showed that PPIMYRC-DOX micelles had a faster drug release efficiency and a higher cumulative drug release in the tumor acid environment than those of normal tissue environments. This phenomenon was owing to the protonation of amino groups on the surface of PPIMYRC-DOX micelles and the increasing electrostatic repulsion in them at low pH in the tumor site. Therefore, we expected that the antitumor effect can be improved due to the controlled release of the drug.

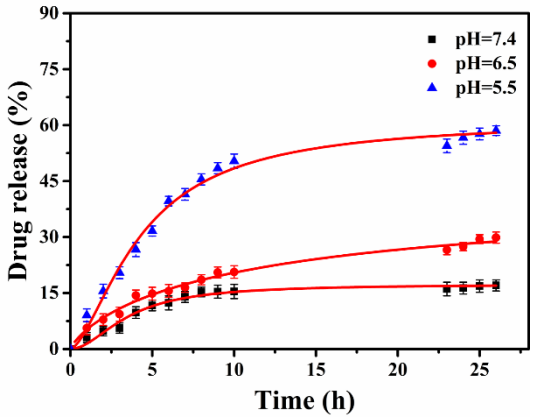

Figure 6. The drug release curve of PPIMYRC-DOX micelles in PBS with pH=7.4, 6.5 and 5.5

3.5 Cytotoxicity assay

The cytotoxicity of PPI and PPIMYRC were studied by MTT assay.[50] As displayed

in **Figure 7A**, when the sample concentration was 440 μg/mL, the relative cellular viability of A549 cells was 78% and 98%, respectively. Besides, as depicted in **Figure 7B**, when the sample concentration was 440 μg/mL, the relative cellular viability of HeLa cells was 84% and 96%, respectively. Therefore, PPI had weak cytotoxicity caused by amino groups on the surface of PPI,[51] PPIMYRC had good biocompatibility and the potential to be used in nanomedicine.

The same method was applied to evaluate the cytotoxicity of free DOX and PPIMYRC-DOX micelles to A549 and HeLa cells. **Figure 7C and 7D** show the results. The higher concentrations of DOX and PPIMYRC-DOX micelles were more toxic. When the DOX concentration was 20 μg/mL, the relative cellular viability of A549 cells incubated with DOX and PPIMYRC-DOX micelles were 37% and 25%, respectively. When the DOX concentration was 20 μg/mL, the relative cellular viability of HeLa cells incubated with DOX and PPIMYRC-DOX micelles were 33% and 28%, respectively.

The experimental results proved that PPIMYRC-DOX micelles had significantly higher cytotoxicity compared with DOX. This may be because DOX passively entered cells through physical diffusion, and PPIMYRC-DOX micelles containing c(RGDfC) may actively enter the cell through endocytosis and release DOX within the cell.[52] However, the cellular uptake mechanism of PPIMYRC-DOX micelles was still unclear and needed further exploration.

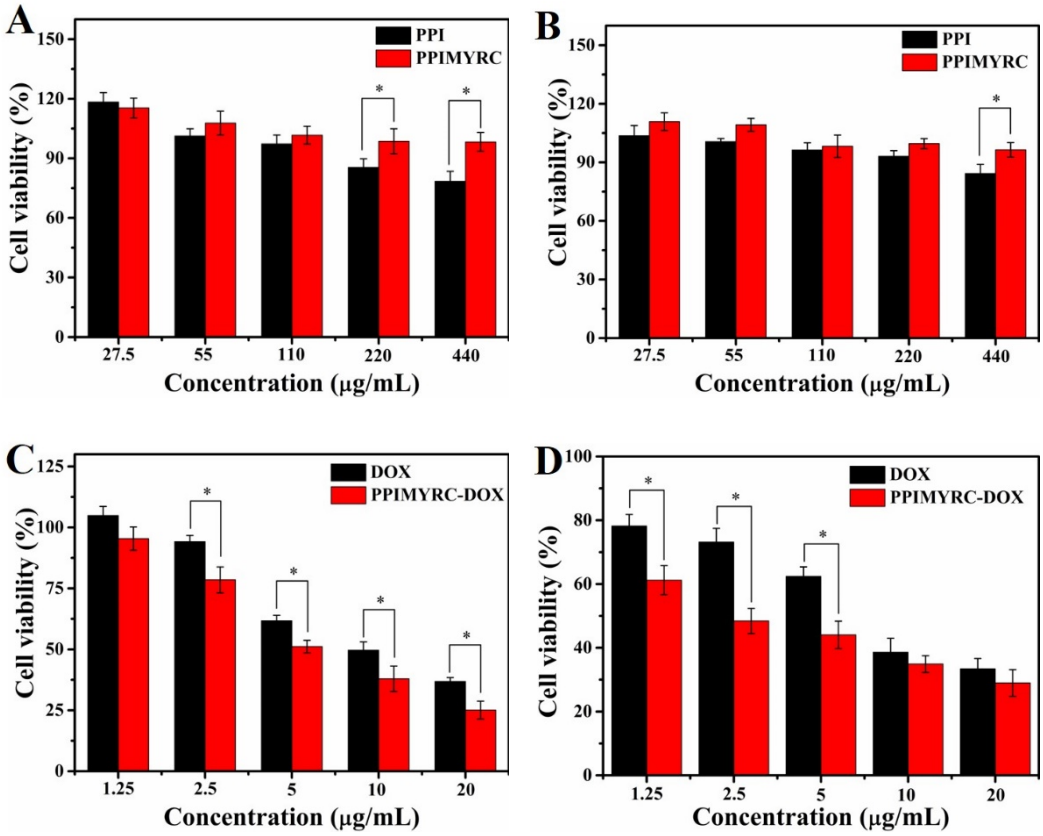

Figure 7. Cell viability of (A) A549 cells and (B) HeLa cells treated with different concentrations of PPI and PPIMYRC micelles, cell viability of (C) A549 cells and (D) HeLa cells treated with different concentrations of DOX and PPIMYRC-DOX micelles. Data are presented as the mean ± SD ($n \geq 3$) (*$P < 0.05$).

3.6 Cellular uptake

The uptake of DOX and PPIMYRC-DOX micelles by A549 cells was characterized by laser confocal microscopy. The nucleus was stained by Hoechst 3342. **Figure 8** showed the fluorescence images of A549 cells incubated with PPIMYRC-DOX micelles and DOX for 20 h, respectively. The red fluorescence in **Figure 8** represented DOX, and the blue fluorescence represented the nucleus. PPIMYRC-DOX micelles

were located inside A549 cells. Under the same exposure time, PPIMYRC-DOX had stronger fluorescence, which indicated that PPIMYRC-DOX micelles were more cytotoxic than free DOX. This is consistent with the results of MTT.

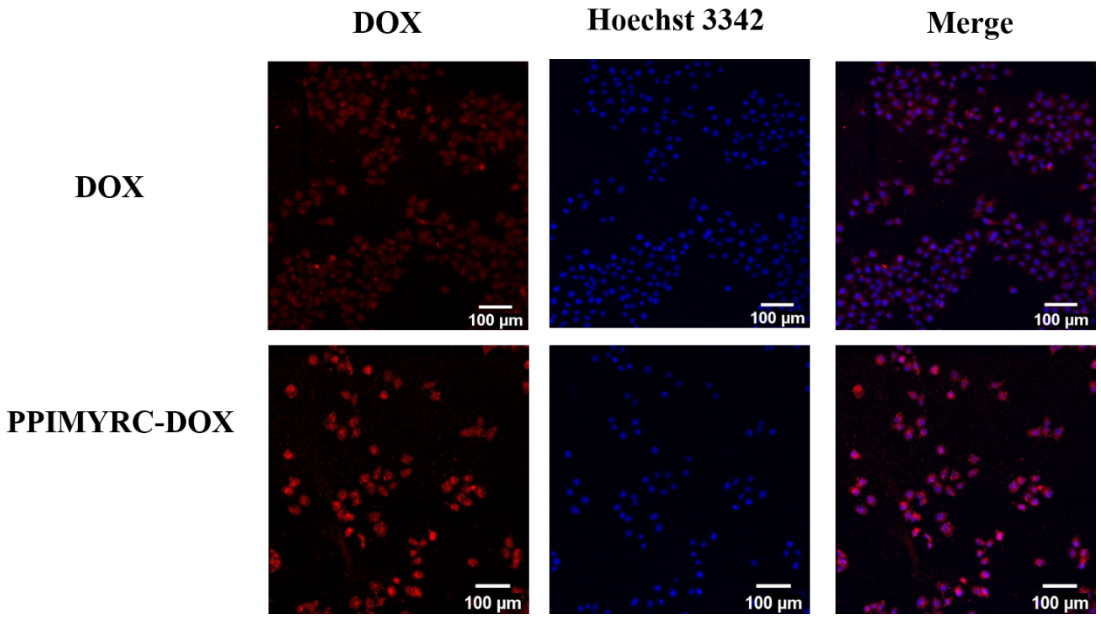

Figure 8. Fluorescence images of A549 cells with free DOX and PPIMYRC-DOX micelles at pH=7.4 for 20 h (C_{DOX}=5 μg/mL)

Meanwhile, flow cytometry was used to analyze the effect of different pH on the cellular uptake of PPIMYRC-DOX micelles. The average fluorescence intensities of DOX and PPIMYRC-DOX micelles were 1590 and 2013 at pH 7.4 in **Figure 9A**, respectively. The cellular uptake of PPIMYRC-DOX micelles was higher than that of free DOX at pH 7.4. This was because DOX diffused into the cells through physical diffusion. Integrin $\alpha_v\beta_3$ is overexpressed in a variety of tumor cells, and short zwitterionic peptide c(RGDfC) can selectively recognize and bind integrin $\alpha_v\beta_3$ with high affinity. Therefore, PPIMYRC-DOX treated cells showed stronger fluorescence.

In addition, the cellular uptake capacity of PPIMYRC-DOX micelles was much higher than that of DOX under acidic conditions. In a weakly acid environment, the amino groups on the surface of PPIMYRC-DOX micelles were protonated, and the micelle surface was positively charged, which caused the enhanced interaction force between PPIMYRC-DOX micelles with the negatively charged cell membrane, so the cellular uptake ability was improved. In addition, the mechanism of PPIMYRC-DOX micelles entering into cells was explored. Genistein, chlorpromazine and amiloride were used to inhibit caveolin-mediated endocytosis, clathrin-related endocytosis and micropinocytosis, respectively. As depicted in **Figure 9B**, the cellular uptake of PPIMYRC-DOX micelles pretreated with chlorpromazine, genistein and amiloride was reduced by 22.43%, 8.75% and 11.64% comparing with the control group, respectively. It was suggested that reticulin-mediated endocytosis was the primary pathway by which PPIMYRC-DOX micelles were primarily taken up by A549 cells, followed by micropinocytosis. Compared with the control group, the cell uptake of PPIMYRC-DOX micelles pretreated with chlorpromazine and amiloride was significantly different from that of the control group. This is related to the integrin ligand c(RGDfC) modified on the surface of PPIMYRC. c(RGDfC) can selectively recognize integrin $\alpha_v\beta_3$ in the extracellular binding domain. Integrin $\alpha_v\beta_3$ can promote the internalization of ligand binding, so that PPIMYRC-DOX can enter target cells through receptor-mediated endocytosis, and release loaded drugs in the cytoplasm.[53,54]

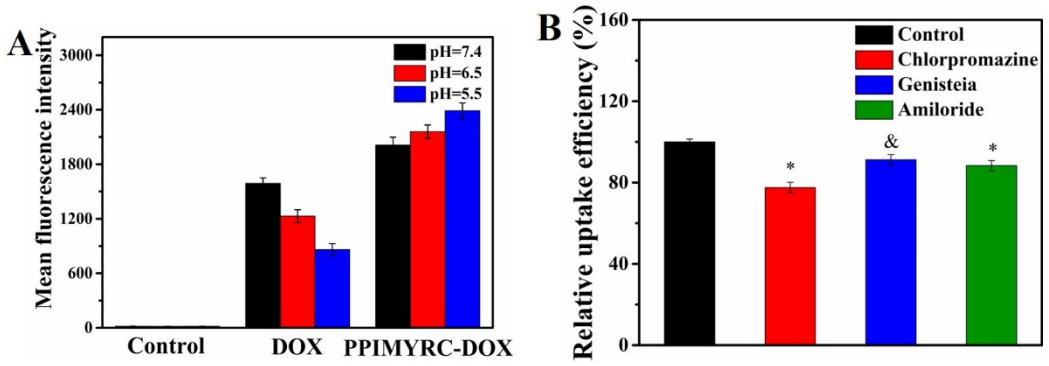

Figure 9. (A) Free DOX and PPIMYRC-DOX micelles incubated in different pH solutions (5.5, 6.5, 7.4) for 20 h, the DOX average fluorescence intensity graph of A549 cells. (B) Relative uptake efficiency of PPIMYRC-DOX micelles incubated with A549 cells for 5 h under various endocytosis inhibitors. * indicates significant differences($^{*}P<0.05$) compared with control group; & indicates no significant differences ($^{\&}P>0.05$) compared with control group.

3.7 Antitumor effect *in vivo*

Due to the excellent results of PPIMYRC-DOX micelles and the good biocompatibility of PPIMYRC *in vitro*, we injected PPIMYRC-DOX micelles into female KM tumor-bearing mice *via* tail vein to evaluate the tumor suppression effect of PPIMYRC-DOX micelles *in vivo*. The weight of the mice was measured at a fixed time in **Figure 10A**. 14 days later, the average body weights of mice in the Saline, DOX, PPIMYRC micelles and PPIMYRC-DOX micelles group were 32.0, 29.1, 31.0 and 31.4 g, respectively. To further assess the inhibitory impact of PPIMYRC-DOX micelles on tumors, the tumor growth recorded at a fixed time was shown in **Figure 10B**. After 2 weeks of treatment, the average tumor volume of the Saline, DOX, PPIMYRC micelles and PPIMYRC-DOX micelles group were calculated to be 726.0,

320.6, 680.4 and 50.4 mm^3, respectively. The average tumor volume of mice in the PPIMYRC-DOX micelles group was about 7% of the tumor volume of the mice in the Saline group, indicating that the tumor inhibition rate of PPIMYRC-DOX micelles was 93%. The photos of the tumor after 14 days were shown in **Figure 10C,** PPIMYRC-DOX micelles had the smallest tumor volume in the experiments, indicating the best tumor-inhibiting effect. This was because PPIMYRC-DOX micelles can accumulate in the tumor site through the EPR effect and targeting effect of c(RGDfC) of PPIMYRC micelles. The good protein stability and small hydrodynamic size were also good for the accumulation in the tumor site.[55] Therefore, PPIMYRC-DOX micelles had a good antitumor effect.

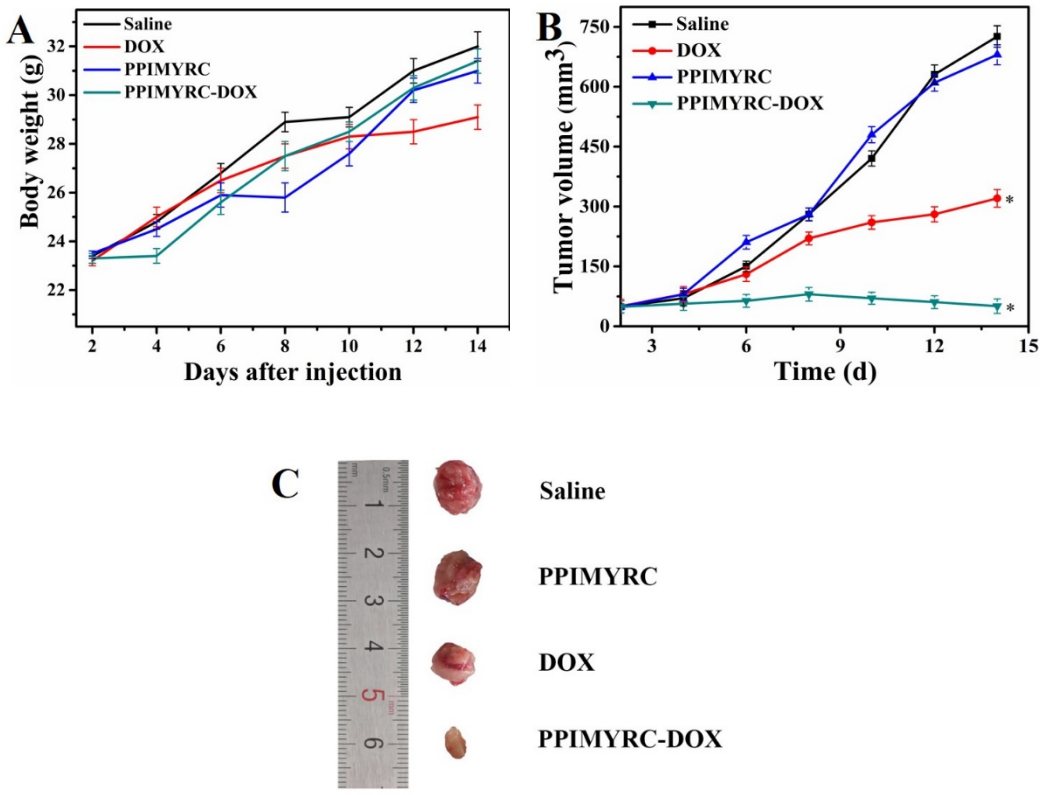

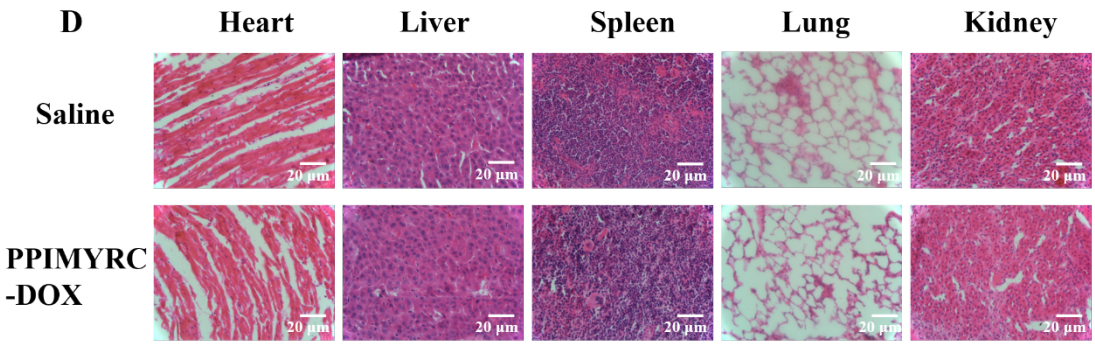

Figure 10. (A) Mice body weight, (B) tumor size changing over time, (C) tumor picture, (D) histological analysis of main organs of mice in Saline group and PPIMYRC-DOX micelles group Tumor-bearing mice were injected with free DOX and PPIMYRC-DOX micelles through the tail vein at a dose of 2.5 mg/kg. * indicates significant differences($^{*}P<0.05$) compared with saline group

In order to analyze the *in vivo* toxicity of PPIMYRC-DOX micelles, hematoxylin-eosin staining was used for histological study. Scholars have found that injection of free DOX will cause certain damage to the heart and liver of mice, including heart myocardial (fibril loss and neutrophil infiltration) and liver damage (congestion and morphological changes).[56] As shown in **Figure 10D**, the tissues of the main organs (heart, liver, spleen, lung, and kidney) of the PPIMYRC-DOX micelles group were similar to the Saline group. In particular, no rupture of myocardial fibers and congestion and morphological changes of liver cells were observed in the heart and liver, indicating that PPIMYRC-DOX micelles had no major organ damage. PPIMYRC-DOX micelles greatly reduced the biological toxicity of DOX. In short, these results confirmed that PPIMYRC-DOX micelles can effectively improve the therapeutic effect of DOX and reduce its systemic toxicity.

4. Conclusion

In summary, we prepared new drug-loaded micelles (PPIMYRC-DOX micelles) based on zwitterionic amphiphilic dendrimers (PPIMYRC) and studied their antitumor effects *in vitro* and *in vivo*. The PPIMYRC used zwitterionic groups and c(RGDfC) modified G2 PPI as the hydrophilic end, N-(2-mercaptoethyl) oleamide as the hydrophobic end. PPIMYRC-DOX micelles had good dispersibility and good protein stability. PPIMYRC-DOX micelles had controlled and pH-responsive release phenomenon. Compared with free DOX, PPIMYRC-DOX micelles had enhanced cytotoxicity and cell uptake at the same concentration. The tumor inhibition rate of the PPIMYRC-DOX micelles group was as high as 93%. The enhanced performance was due to the zwitterionic and targeting property of PPIMYRC-DOX micelles. Moreover, PPIMYRC-DOX micelles did not cause damage to the major organs of mice. Therefore, PPIMYRC-DOX micelles improved the tumor inhibition effect and reduced the side effects of DOX. We provide a new method for nano-drug delivery systems.

Funding:

This research was funded by Natural Science Foundation of Hebei Province (B2017203229, H2022203004) and Subsidy for Hebei Key Laboratory of Applied Chemistry after Operation Performance (22567616H).

Conflicts of Interest: The authors declare no conflict of interest.

AUTHOR INFORMATION

Corresponding Author

Notes: **xyzhang05@126.com**; **lgwang@ysu.edu.cn**

Supporting Information

Materials, detailed synthesis steps and dosages of zwitterionic dendrimer, ^{1}H NMR spectrum of c(RGDfC), and GPC elution curve of PPIMYRC.

Reference

(1) Cao, W.; Chen, H. D.; Yu, Y. W.; Li, N.; Chen, W. Q. Changing profiles of cancer burden worldwide and in China: a secondary analysis of the global cancer statistics 2020. *Chin. Med. J.* **2021**, 134 (7), 783-791.

(2) Sung, H.; Ferlay, J.; Siegel, R. L.; Laversanne, M.; Soerjomataram, I.; Jemal, A.; Bray, F. Global cancer statistics 2020: GLOBOCAN estimates of incidence and mortality worldwide for 36 cancers in 185 countries. *CA. Cancer. J. Clin.* **2021**, 71 (3), 209-249.

(3) Arnold, M.; Abnet, C. C.; Neale, R. E.; Vignat, J.; Giovannucci, E. L.; McGlynn, K. A.; Bray, F. Global burden of 5 major types of gastrointestinal cancer. *Gastroenterology* **2020**, 159 (1), 335.

(4) Gong, F.; Yang, N. L.; Wang, X. W.; Zhao, Q.; Chen, Q.; Liu, Z.; Cheng, L. Tumor microenvironment-responsive intelligent nanoplatforms for cancer theranostics. *Nano Today* **2020**, 32,100851.

(5) Li, J. Y.; Chen, Y. P.; Li, Y. Q.; Liu, N.; Ma, J., Chemotherapeutic and targeted agents can modulate the tumor microenvironment and increase the efficacy of immune checkpoint blockades. *Mol. Cancer.* **2021**, 20 (1),27.

(6) Borghese, C.; Casagrande, N.; Corona, G.; Aldinucci, D., Adipose-derived stem cells primed with paclitaxel inhibit ovarian cancer spheroid growth and overcome

paclitaxel resistance. *Pharmaceutics* **2020**, 12 (5),401.

(7) Zhao, G. F.; Sun, Y.; Dong, X. Y. Zwitterionic polymer micelles with dual conjugation of doxorubicin and curcumin: synergistically enhanced efficacy against multidrug-resistant tumor cells. *Langmuir* **2020**, 36 (9), 2383-2395.

(8) Zhou, Z. J.; Du, C.; Zhang, Q. Y.; Yu, G. C.; Zhang, F. W.; Chen, X. Y., Exquisite vesicular nanomedicine by paclitaxel mediated co-assembly with camptothecin prodrug. *Angew. Chem. Int. Ed. Engl.* **2021**, 60 (38), 21033-21039.

(9) Avramovic, N.; Mandic, B.; Savic-Radojevic, A.; Simic, T., Polymeric nanocarriers of drug delivery systems in cancer therapy. *Pharmaceutics* **2020**, 12 (4), 124804.

(10) Khan, M. M.; Filipczak, N.; Torchilin, V. P., Cell penetrating peptides: A versatile vector for co-delivery of drug and genes in cancer. *J. Controll. Release.* **2021**, 330, 1220-1228.

(11) Ren, L. F.; Lv, J.; Wang, H.; Cheng, Y. Y., A coordinative dendrimer achieves excellent efficiency in cytosolic protein and peptide delivery. *Chem. Int. Ed. Engl.* **2020**, 59 (12), 4711-4719.

(12) Das, S.; Lazenby, R. A.; Yuan, Z.; White, R. J.; Park, Y. C. Effect of laser irradiation on reversibility and drug release of light-activatable drug-encapsulated liposomes. *Langmuir* **2020**, 36 (13), 3573-3582.

(13) Guo, Q. L.; Zhang, L.; He, M. M.; Jiang, X. H.; Tian, J. R.; Li, Q. R.; Liu, Z. W.; Wang, L. G.; Sun, H. T., Doxorubicin-loaded natural daptomycin micelles with enhanced targeting and anti-tumor effect in vivo. *Eur. J. Med. Chem.* **2021**, 222, 113582.

(14) Yuan, Z. F.; Li, B. W.; Gu, W. C.; Luozhong, S.; Li, R. X.; Jiang, S. Y. Mitigating the Immunogenicity of AAV-Mediated Gene Therapy with an Immunosuppressive Phosphoserine-Containing Zwitterionic Peptide. *JACS* **2022**, 144 (44), 20507-20513.

(15) Ghosh, B.; Biswas, S., Polymeric micelles in cancer therapy: State of the art. *J. Control. Release.* **2021**, 332, 127-147.

(16) Liu, W. W.; Li, J. J.; Qin, Z. H.; Yao, M. M.; Tian, X. L.; Zhang, Z. M.; Zhang, L.; Guo, Q.; Zhang, L. H.; Zhu, D. W.; et al. Zwitterionic unimolecular micelles with pH and temperature response: Enhanced in vivo circulation stability and tumor therapeutic efficiency. *Langmuir* **2020**, 36 (13), 3356-3366.

(17) Cai, H.; Tan, P.; Chen, X. T.; Kopytynski, M.; Pan, D. Y.; Zheng, X. L.; Gu, L.; Gong, Q. Y.; Tian, X. H.; Gu, Z. W.; et al. Stimuli-sensitive linear-dendritic block copolymer-drug prodrug as a nanoplatform for tumor combination therapy. *Adv. Mater.* **2022**, 34 (8).

(18) Huang, D.; Sun, L. N.; Huang, L.; Chen, Y. Z., Nanodrug delivery systems modulate tumor vessels to increase the enhanced permeability and retention effect. *J. Pers. Med.* **2021**, 11 (2),124.

(19) Fang, J.; Islam, W.; Maeda, H., Exploiting the dynamics of the EPR effect and strategies to improve the therapeutic effects of nanomedicines by using EPR effect enhancers. *Adv. Drug Deliv. Rev.* **2020**, 157, 142-160.

(20) Wang, J.; Li, B. X.; Huang, D.; Norat, P.; Grannonico, M.; Cooper, R. C.; Gui, Q.; Chow, W. N.; Liu, X. R.; Yang, H. Nano-in-nano dendrimer gel particles for efficient topical delivery of antiglaucoma drugs into the eye. *Chem. Eng. J.* **2021**, 425.

(21) Chen, S. Q.; Zhong, Y.; Fan, W. F.; Xiang, J. J.; Wang, G. W.; Zhou, Q.; Wang, J. Q.; Geng, Y.; Sun, R.; Zhang, Z.; et al. Enhanced tumour penetration and prolonged circulation in blood of polyzwitterion-drug conjugates with cell-membrane affinity. *Nat. Biomed. Eng.* **2021**, 5 (9), 1019-1037.

(22) Lv, J.; Wang, C. P.; Li, H. R.; Li, Z.; Fan, Q. Q.; Zhang, Y.; Li, Y. W.; Wang, H.; Cheng, Y. Y. Bifunctional and bioreducible dendrimer bearing a fluoroalkyl tail for efficient protein delivery both in vitro and in vivo. *Nano Letters* **2020**, 20 (12), 8600-8607.

(23) Yang, W.; Liu, S. J.; Bai, T.; Keefe, A. J.; Zhang, L.; Ella-Menye, J. R.; Li, Y. T.; Jiang, S. Y., Poly(carboxybetaine) nanomaterials enable long circulation and prevent polymer-specific antibody production. *Nano Today* **2014**, 9 (1), 10-16.

(24) Wu, J.; Zhao, C.; Hu, R. D.; Lin, W. F.; Wang, Q. M.; Zhao, J.; Bilinovich, S. M.; Leeper, T. C.; Li, L. Y.; Cheung, H. M.; Chen, S. F.; Zheng, J., Probing the weak interaction of proteins with neutral and zwitterionic antifouling polymers. *Acta. Biomater.* **2014**, 10 (2), 751-760.

(25) Liang, Y.; Li, H. C.; Fan, L. Y.; Li, R. Y.; Cui, Y. S.; Ji, X. B.; Xiao, H. Y.; Hu, J.; Wang, L. G., Zwitterionic daptomycin stabilized palladium nanoparticles with enhanced peroxidase-like properties for glucose detection. *Colloids. Surf. A.* **2022**, 633,127797.

(26) Li, R. Y.; Fan, L. Y.; Chen, S. F.; Wang, L. G.; Cui, Y. S.; Ma, G. L.; Zhang, X. Y.; Liu, Z. W. Zwitterionic sulfhydryl sulfobetaine stabilized platinum nanoparticles for enhanced dopamine detection and antitumor ability. *Acs Appl. Mater. Interfaces* **2022**,

14 (49), 55201-55216.

(27) Zheng, G. Q.; Liu, S.; Zha, J. Q.; Zhang, P.; Xu, X. W.; Chen, Y. T.; Jiang, S. Y., Protecting enzymatic activity via zwitterionic nanocapsulation for the removal of phenol compound from wastewater. *Langmuir* 2019, 35 (5), 1858-1863.

(28) Li, Q. S.; Wen, C. Y.; Yang, J.; Zhou, X. C.; Zhu, Y. N.; Zheng, J.; Cheng, G.; Bai, J.; Xu, T.; Ji, J.; et al. Zwitterionic Biomaterials. *Chem. Rev.* **2022**, 122 (23), 17073-17154.

(29) Wang, D. Y.; Yang, G.; van der Mei, H. C.; Ren, Y. J.; Busscher, H. J.; Shi, L. Q., Liposomes with water as a pH-responsive functionality for targeting of acidic tumor and infection sites. *Angew. Chem. Int. Ed. Engl.* **2021**, 60 (32), 17714-17719.

(30) Wang, L. G.; Zhu, L. L.; Bernards, M. T.; Chen, S. F.; Sun, H. T.; Guo, X. L.; Xue, W. L.; Cui, Y. S.; Gao, D. W., Dendrimer-based biocompatible zwitterionic micelles for efficient cellular internalization and enhanced antitumor effects. *ACS. Appl. Polym. Mater.* **2020**, 2 (2), 159-171.

(31) Phan, Q. T.; Patil, M. P.; Tu, T. T. K.; Kim, G. D.; Lim, K. T., Synthesis of zwitterionic redox-responsive nanogels by one-pot amine-thiol-ene reaction for anticancer drug release application. *React. Funct. Polym.* **2020**, 147, 104463.

(32) Wei, T.; Chen, C.; Liu, J.; Liu, C.; Posocco, P.; Liu, X. X.; Cheng, Q.; Huo, S. D.; Liang, Z. C.; Fermeglia, M.; Pricl, S.; Liang, X. J.; Rocchi, P.; Peng, L., Anticancer drug nanomicelles formed by self-assembling amphiphilic dendrimer to combat cancer drug resistance. *Proc. Natil. Acad. Sci. U. S. A.* **2015**, 112 (10), 2978-2983.

(33) Tang, J. Z.; Huang, N.; Zhang, X.; Zhou, T.; Tan, Y.; Pi, J. L.; Pi, L.; Cheng, S.;

Zheng, H. Z.; Cheng, Y. Aptamer-conjugated PEGylated quantum dots targeting epidermal growth factor receptor variant III for fluorescence imaging of glioma. *Int. J. Nanomedicine* **2017**, 12, 3899-3911.

(34) Xia, Y.; Xu, T. T.; Wang, C. B.; Li, Y. H.; Lin, Z. F.; Zhao, M. Q.; Zhu, B., Novel functionalized nanoparticles for tumor-targeting co-delivery of doxorubicin and siRNA to enhance cancer therapy. *Int. J. Nanomedicine.* **2018**, 13, 143-159.

(35) Chen, Y. J.; Jia, L. X.; Zhu, G. L.; W, W.; G, M.; L, H. X.; Z, Y.; Z, M. H.; Z, F. Y.; C, X. Z., Sortase A-mediated cyclization of novel polycyclic RGD peptides for αvβ3 integrin targeting. *Bioorg. Med. Chem. Lett.* **2022**, 73, 128888.

(36) Liu, X. Y.; Cui, W. G.; Li, B.; Hong, Z., Targeted therapy for glioma using cyclic RGD-entrapped polyionic complex nanomicelles. *Int. J. Nanomedicine.* **2012**, 7, 2853-2862.

(37) Zheng, P.; Liu, Y.; Chen, J. J.; Xu, W. G.; Li, G.; Ding, J. X., Targeted pH-responsive polyion complex micelle for controlled intracellular drug delivery. *Chin. Chem. Lett.* 2020, 31 (5), 1178-1182.

(38) Zhang, L. P.; Xi, L.; Shi, G.; Zhu, C. P.; Ni, C. H., Reduction-responsive zwitterionic nanogels based on carboxymethyl chitosan for enhancing cellular uptake in drug release. *Colloid. Polym. Sci.* **2016**, 294 (3), 629-637.

(39) Lu, Y.; Yue, Z. G.; Xie, J. B.; Wang, W.; Zhu, H.; Zhang, E. S.; Cao, Z. Q., Micelles with ultralow critical micelle concentration as carriers for drug delivery. *Nat. Biomed. Eng.* **2018**, 2 (5), 318-325.

(40) Li, R.; Zhao, Y.; Zhang, T.; Ju, Z.; Ji, X.; Cui, Y.; Wang, L.; Xiao, H. Pd

nanoparticles stabilized by bitter gourd polysaccharide with peroxidase properties for H_2O_2 detection. *Int.J. Biol. Macromol.* **2023**, 233, 123513.

(41) Xue, W. L.; Trital, A.; Liu, S. H.; Xu, L. B., Doxorubicin-loaded micelles with high drug-loading capacity and stability based on zwitterionic oligopeptides. *New. J. Chem.* **2020**, 44 (29), 12633-12638.

(42) Bai, T.; Shao, D. Y.; Chen, J. X.; Li, Y. F.; Xu, B.; Kong, J., pH-responsive dithiomaleimide-amphiphilic block copolymer for drug delivery and cellular imaging. *J. Colloid. Interface Sci.* **2019**, 552, 439-447.

(43) He, J. F.; Wang, J.; Gao, S. B.; Cui, Y. S.; Ji, X. B.; Zhang, X. Y.; Wang, L. G., Biomineralized synthesis of palladium nanoflowers for photothermal treatment of cancer and wound healing. *Int. J. Pharm.* **2022**, 615, 121489.

(44) Dong, L.; Li, R. Y.; Wang, L. Q.; Lan, X. F.; Sun, H. T.; Zhao, Y.; Wang, L. G., Green synthesis of platinum nanoclusters using lentinan for sensitively colorimetric detection of glucose. *Int. J. Biol. Macromol.* **2021**, 172, 289-298.

(45) Zhu, J. W.; Tian, J.; Yang, C.; Chen, J. P.; Wu, L. H.; Fan, M. N.; Cai, X. J. L-arg-rich amphiphilic dendritic peptide as a versatile NO donor for NO/Photodynamic synergistic treatment of bacterial infections and promoting wound healing. *Small* **2021**, 17 (32).

(46) Xu, J. C.; Zhang, J.; Xiong, D.; Lin, W. J.; Wen, L. Y.; Zhang, L. J., Enhanced stability of crosslinked and charged unimolecular micelles from multigeometry triblock copolymers with short hydrophilic segments: dissipative particle dynamics simulation. *Eur. Phys. J. E. Soft. Matter.* **2019**, 15 (4), 546-558.

(47) Yang, W. J.; Zhang, F. W.; Deng, H. Z.; Lin, L. S.; Wang, S.; Kang, F.; Yu, G. C.; Lau, J.; Tian, R.; Zhang, M. R.; Wang, Z. T.; He, L. C.; Ma, Y.; Niu, G.; Hu, S.; Chen, X. Y., Smart nanovesicle-mediated immunogenic cell death through tumor microenvironment modulation for effective photodynamic immunotherapy. *ACS Nano* **2020**, 14 (1), 620-631.

(48) Zhou, Z. J.; Wang, Y. T.; Yan, Y.; Zhang, Q.; Cheng, Y. Y., Dendrimer-templated ultrasmall and multifunctional photothermal agents for efficient tumor ablation. *ACS Nano* **2016**, 10 (4), 4863-4872.

(49) Deirram, N.; Zhang, C. H.; Kermaniyan, S. S.; Johnston, A. P. R.; Such, G. K., pH-responsive polymer nanoparticles for drug delivery. *Macromol. Rapid. Commun.* **2019**, 40 (10), 1800917.

(50) He, J. F.; Yu, S. Q.; Ma, Z. Y.; Sun, H. T.; Yang, Q. H.; Liu, Z. W.; Wang, X.; Zhang, X. Y.; Wang, L. G. Polymyxin E biomineralized and doxorubicin-loaded gold nanoflowers nanodrug for chemo-photothermal therapy. *Int. J. Pharm.* **2022**, 625.

(51) Zhou, L. Y.; Zhu, Y. H.; Wang, X. Y.; Shen, C.; Wei, X. W.; Xu, T.; He, Z. Y., Novel zwitterionic vectors: Multi-functional delivery systems for therapeutic genes and drugs. *Comput. Struct. Biotechnol. J.* **2020**, 18, 1980-1999.

(52) Liu, G. Y.; Luo, Q. Q.; Gao, H. Q.; Chen, Y.; Wei, X.; Dai, H.; Zhang, Z. C.; Ji, J., Cell membrane-inspired polymeric micelles as carriers for drug delivery. *Biomater. Sci.* **2015**, 3 (3), 490-499.

(53) Torcasio, S. M.; Oliva, R.; Montesi, M.; Panseri, S.; Bassi, G.; Mazzaglia, A.; Piperno, A.; Coulembier, O.; Scala, A. Three-armed RGD-decorated starPLA-PEG

nanoshuttle for docetaxel delivery. *Biomater. Adv.* **2022**, 140.

(54) Battistini, L.; Bugatti, K.; Sartori, A.; Curti, C.; Zanardi, F. RGD peptide-drug conjugates as effective dual targeting platforms: recent advances. *Eur. J. Org. Chem.* **2021**, 2021 (17), 2506-2528.

(55) Xia, Y.; Tang, G. Y.; Guo, M.; Xu, T. T.; Chen, H. Y.; Lin, Z. F.; Li, Y. H.; Chen, Y.; Zhu, B.; Liu, H. S.; Cao, J., Silencing KLK12 expression via RGDfC-decorated selenium nanoparticles for the treatment of colorectal cancer in vitro and in vivo. *Mat. Sci. Eng. C-Mater.* **2020**, 110, 110594.

(56) Gabizon, A.; Meshorer, A.; Barenholz, Y. Comparative long-term study of the toxicities of free and liposome-associated doxorubicin in mice after intravenous administration. *J. Natl. Cancer Inst.* **1986**, 77 (2), 459-469.

TOC